

Role of Nanoparticle Geometry in Endocytosis: Laying Down to Stand Up

Changjin Huang,[†] Yao Zhang,[†] Hongyan Yuan,^{‡,||} Huajian Gao,[‡] and Sulin Zhang^{*,†,§}

[†]Department of Engineering Science and Mechanics, The Pennsylvania State University, University Park, Pennsylvania 16802, United States

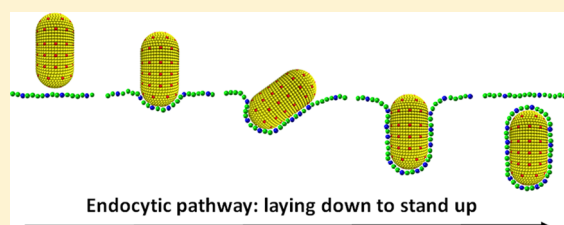
[‡]School of Engineering, Brown University, Providence, Rhode Island 02912, United States

[§]Department of Bioengineering, The Pennsylvania State University, University Park, Pennsylvania 16802, United States

S Supporting Information

ABSTRACT: Nanoparticles (NPs) hold great promises for targeted disease diagnosis and therapy. Despite considerable progress in biomimetic design of NP-bioconjugates, the roles of NP size and shape in endocytosis are still not fully understood. Using an efficient coarse-grained molecular dynamics (CGMD) model, we simulate receptor-mediated endocytosis of NPs of various sizes and shapes. Our simulations demonstrate that both NP size and shape modulate the kinetics of endocytosis. For spherical NPs, there exists an optimal size at which endocytosis takes the shortest time. For a spherocylindrical NP with the initial upright docking position on the membrane plane, endocytosis proceeds through a laying-down-then-standing-up sequence. A free energy analysis reveals that NP size primarily determines whether endocytosis can complete, while NP shape breaks the symmetry of curvature energy landscape and hence dictates the endocytic pathway and the angle of entry. The findings shed light on the rational design of NP-based diagnostic and therapeutic agents with improved cellular targeting.

KEYWORDS: Nanoparticle, shape, endocytosis, molecular dynamics, cancer therapy



Receptor-mediated endocytosis is a process by which cells engulf and internalize nanometer-sized targets, driven by the specific binding of the ligands on the surface of targets with the receptors on the cell membrane. Examples of targets range from viruses^{1–4} to synthetic nanoparticles (NPs)^{5–8} for disease diagnosis and therapy, both of which vary widely in size and shape. With such diversified NPs, a fundamental question arises regarding how target size and geometry regulate endocytosis. In vitro experimental studies have demonstrated that both target size and shape influence the kinetics of endocytosis, and there exist an optimal size and shape at which cellular uptake maximizes.^{4,9–12} The underlying mechanisms responsible for the size and shape effects are, however, not fully understood. Analytical models^{13–20} have been primarily focused on spherical targets because of the complexity in calculating the membrane bending energy for nonspherical targets, particularly when the membrane is under tension. Computational models may, in theory, simulate endocytosis of targets of any geometry.^{21–23} However, owing to the high computational costs, existing numerical models often use very high ligand and receptor densities in order to accelerate the simulations. This imposes unrealistic driving force for endocytosis, and therefore creating an incomplete, or sometimes even inaccurate, picture of endocytic kinetics. As a result, the roles of target size and shape in endocytosis, and whether the roles are interrelated or separable, remain largely unknown.

We herein report that, using a highly effective coarse-grained model, both target size and shape modulate the kinetics of

endocytosis. In general, endocytosis proceeds by simultaneous membrane wrapping and NP rotation. Our simulations and analyses show for the first time that size mainly determines whether endocytosis can complete, while shape breaks the symmetry of curvature energy landscapes and therefore dictates the endocytic pathways and the angle of entry. In addition to presenting a coarse-grained molecular dynamics (CGMD) model for the endocytosis of NPs, we map out the endocytic pathways of spherocylindrical NPs through local energy analyses. Our findings regarding the NP size and shape effects on endocytosis suggest design principles of NP-based therapeutics with optimized cellular targeting.

Our membrane model²⁴ consists of coarse-grained lipid agents that are stabilized in a two-dimensional (2D) fluid surface in 3D space using an anisotropic pairwise interagent potential. The one-agent-thick coarse-grained model improves the computational efficiency by at least an order of magnitude compared to the chain-of-bead models,^{21,25,26} while faithfully captures both the in-plane viscosity and out-of-plane bending rigidity of cell membranes. The interagent interaction potential yields a membrane bending rigidity of $\kappa = 25 k_B T$ and the diffusivity of $D = 0.06 \sigma^2/\tau$, where $k_B T$ is the thermal energy, T is the temperature, and $\sigma \sim 2$ nm and $\tau \sim 0.1$ μ s are,

Received: July 16, 2013

Revised: August 21, 2013

respectively, the characteristic length and time scales of the model. A planar membrane consisting of $\sim 60\,000$ lipid agents is preassembled under periodic boundary conditions. CGMD simulations are performed in the $N\Sigma T$ ensemble, where N is the total number of the coarse-grained agents. The membrane is maintained at zero tension ($\Sigma = 0$) using a modified Berendsen pressure coupling algorithm.²⁴ The simulations include a population of sparsely scattered, diffusive membrane-bound receptors, which can specifically bind to the ligands immobilized on the NP surface with a binding energy of $\mu = 60k_B T$ and a capture radius of $R_{\text{cut}} = 15\sigma$ (see Figure 1). In the

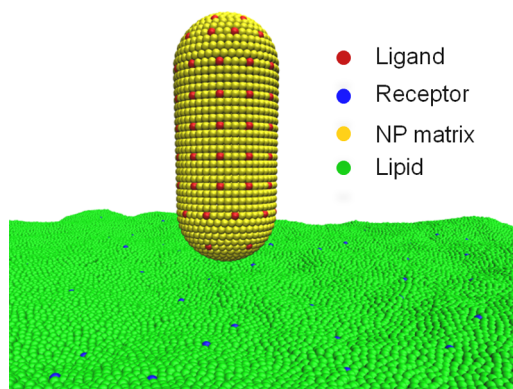


Figure 1. The CGMD model of receptor-mediated endocytosis. Lipid bilayer membrane is coarse-grained by one-agent-thick (green) aggregates with sparsely scattered receptors (blue). The NP is modeled by a particle assembly (yellow) with ligands (red) immobilized on its surface.

simulations, the ligand density on the NP and the receptor density in the membrane are set to be $\xi_L = 0.059/\sigma^2$ and $\xi_R = 0.0038/\sigma^2$, respectively, which are on the same order of magnitude as the ligand and receptor densities in real biological systems.^{27–29} A more detailed description of the model and the simulation method is given in Supporting Information.

To systematically investigate the effects of NP size and shape on the kinetics of endocytosis, we use both spherical NPs with different radii and spherocylindrical NPs with different aspect ratios in our simulations. The aspect ratio of the spherocylindrical NPs is defined as $\rho = (R + 0.5L)/R$, where R and L are the radius of the hemispherical caps at both ends and the length of the cylindrical portion, respectively. The spherocylindrical NPs are reminiscent of capped carbon nanotubes. Figure 2 depicts the snapshots of the endocytic process of the NPs. The NPs are initially docked on the pre-equilibrated membrane, with their long axes of the spherocylindrical NPs normal to the membrane surface ($\theta = 90^\circ$). Ligand–receptor binding drives membrane invagination of the NPs. After the NP is substantially wrapped, the membrane necks. In the final stage, the membrane pinches off and endocytosis completes.

An interesting observation is the symmetry breaking in the invagination process of the spherocylindrical NPs. For $\rho = 1.5$, the NP slightly tilts by an angle of $\sim 20^\circ$ from its initial upright docking position after invagination starts. Endocytosis of the NP then proceeds at this angle until the NP is fully internalized. The invagination pathway of the spherocylindrical NP of a larger aspect ratio ($\rho = 2$) involves two symmetry-breaking processes. From its initial upright docking position, the NP continues rotating until it completely lays down on the membrane surface. The NP then stands up and is finally

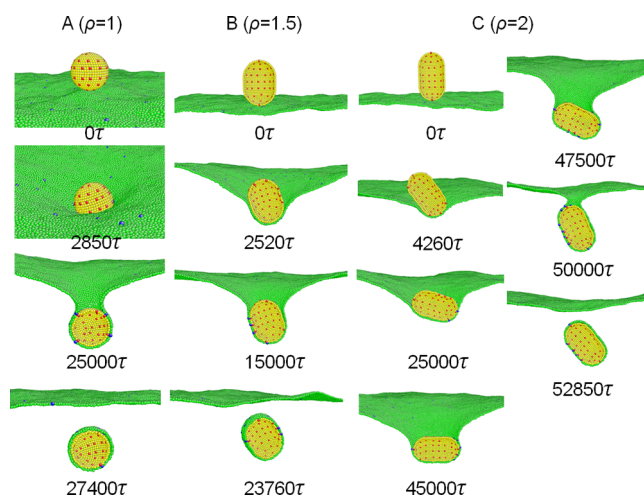


Figure 2. Representative simulation snapshots showing the endocytic pathways of NPs with different aspect ratios. The front half of the membrane model is not shown in the figures for the clarity of visualization. For all the cases shown, $R = 10.0\sigma$. (A) $\rho = 1$ (spherical); (B) $\rho = 1.5$; (C) $\rho = 2$.

internalized with a nearly 90° entry angle. We have simulated endocytosis of spherocylindrical NPs for $\rho > 2$ and observed that such lying-down-then-standing-up sequence appears to be a universal pathway. Additional simulations demonstrate that the standing-up process is absent provided that very high ligand and receptor densities are prescribed, consistent with recent CGMD simulations²³ wherein a lipid molecule is coarse-grained by three connected beads.²⁵ This may be due to the loss of interaction specificity at high ligand/receptor densities or to the momentum for NP internalization created by the unrealistically high driving force of ligand–receptor binding.

We quantify the kinetics of endocytosis by the wrapped areal fraction of the NP (f) with respect to the endocytic time. For spherical NPs, our simulations show that at a small NP size ($R = 5.0\sigma$), the NP can only be partially wrapped ($\sim 50\%$). Partial wrapping proceeds via a series of thermally assisted barrier-crossing events, as explained in Supporting Information. At an intermediate NP size ($R = 7.5\sigma$), endocytosis completes fastest. Further increasing the NP size slows down endocytosis monotonically. Such trends are consistent with the existing analytical and experimental results.^{9,11,14,18,30} Figure 3b shows the effect of the aspect ratio on the endocytic time of the NPs with the same radius ($R = 10.0\sigma$). All the spherocylindrical NPs can be fully endocytosed. The spherical NP takes longer time to be fully endocytosed than the spherocylindrical NP of $\rho = 1.5$, but shorter time than the spherocylindrical NP of $\rho = 2$. Further increasing ρ leads to increasing endocytic time, owing to the increasing number of diffusive receptors participated in the wrapping since endocytosis is limited by the diffusion of the receptors. For all the cases shown in Figure 3, wrapping slows down following an initially rapid wrapping regime. This observation is consistent with the parabolic rate law ($R \propto t^{1/2}$) of wrapping predicted by a previous theory.¹⁴ We further note that for the spherocylindrical NP with $\rho = 2$ the wrapped area sharply increases to 35% at the beginning of wrapping. Such a sharp wrapping area increase indicates a contact instability, corresponding to the laying-down process from its initial upright position, as observed in Figure 2.

We next rationalize the energetics of endocytosis and its implications to the completion of endocytosis and the

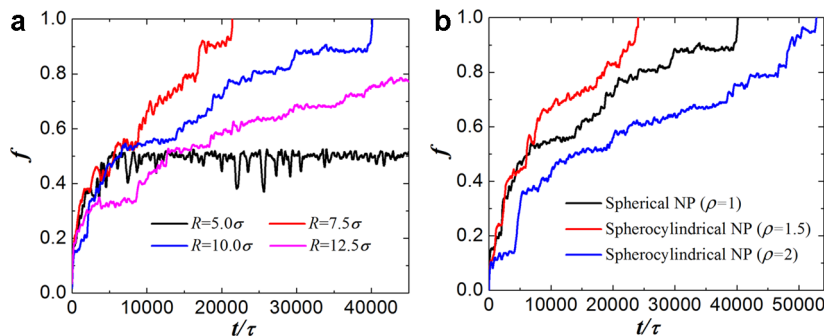


Figure 3. Effects of NP size and shape on the endocytic time. (a) Evolution of the areal wrapping fraction (f) of spherical NPs with various radii; (b) evolution of the areal wrapping fraction of NPs with the same radius ($R = 10.0\sigma$) but different aspect ratios. In the simulations, the spherocylindrical NPs are initially docked on the membrane with their long axes perpendicular to the membrane.

endocytic pathways. Membrane invagination of an NP involves both bending and tension energy penalties. The relative significance of bending and tension defines a characteristic NP size $\lambda = (\kappa/\Sigma)^{1/2}$ below which the curvature energy is dominant. For typical values of κ and Σ ,³¹ the characteristic NP diameter is ~ 100 nm. Membrane tension can be negligible in some physiologically relevant conditions, such as when large-scale membrane reservoirs are available and able to release.³² In the tension-free condition, the curvature energy of the membrane adhering to the entire NP accounts for the total energy penalty. From a global thermodynamics point of view, endocytosis can complete only if the total adhesion energy exceeds the bending penalty for internalizing the NP. For a spherocylindrical NP with an aspect ratio of ρ , this global energy balance criterion defines a lower limit of NP radius $R_0 = [(3+\rho)\kappa/(2\rho\mu\xi_1)]^{1/2}$ for the completion of endocytosis (see Supporting Information). For $\rho = 1$ (a spherical NP), $R_0 = [2\kappa/(\mu\xi_1)]^{1/2} \approx 3.8\sigma$, which is slightly smaller than the threshold radius (5σ) identified by the direct numerical simulations, indicating a secondary mechanism that regulates the threshold value, as discussed in Supporting Information. With increasing ρ , R_0 monotonically decreases, which indicates that a spherocylindrical NP with a larger aspect ratio is easier to be endocytosed. We note when ρ varies from 1 (a spherical NP) to ∞ (a 1D rod), R_0 decreases by only two folds (see Supporting Information), suggesting that the aspect ratio only plays a secondary role in the completion of endocytosis.

Our CGMD simulations show that NP endocytosis is comprised of a sequence of simultaneous membrane wrapping and NP rotation. To map out the sequence, that is, the endocytic pathways, we next compute the relative thermodynamic resistance force at different wrapping angles. Membrane bending energy for a partially wrapped NP includes contributions from two parts: the curvature energy of adherent portion and of the free curved membrane detaching from the adherent point. For a nonspherical NP, the curvature energy $E_b(f;\theta)$ is generally a function of the wrapping angle θ and the wrapped areal fraction f . Assuming the system reaches a thermodynamic equilibrium after each binding event of a ligand–receptor pair, the curvature energy of the free curved membrane vanishes (with a vanishing mean curvature) in the tensionless limit. Under this condition, the curvature energy of the membrane adhered to the NP accounts for the total energy penalty, which is analytically available. In Figure 4, the solid lines plot the curvature energy profiles for the NP ($\rho = 2$) wrapped with two fixed wrapping angles, $\theta = 0^\circ$ (horizontally) and $\theta = 90^\circ$ (vertically). The analytical energy profiles agree

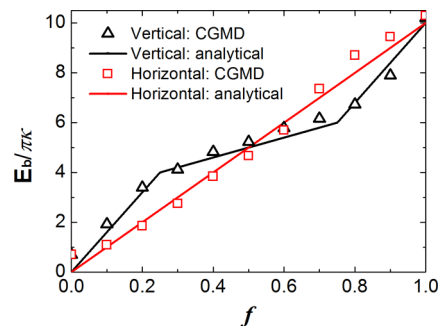


Figure 4. Bending energy profiles for internalizing a spherocylindrical NP ($\rho = 2$) with different wrapping angles (red, $\theta = 0^\circ$, that is, its long axis is parallel to the membrane plane; black, $\theta = 90^\circ$, that is, its long axis is normal to the membrane plane).

very well with the CGMD simulations, denoted by symbols. The curvature energies linearly scale with the wrapped areal fraction for both the wrapping angles $\theta = 0^\circ$ and $\theta = 90^\circ$. However, for $\theta = 90^\circ$ the linear curve is constituted of three segments of different slopes. Because the two wrapping angles represent the extremes, these two curves envelope the curvature energy profiles of all the other wrapping angles.

The energy profiles plotted in Figure 4 indicate the endocytic pathways. At a small wrapping extent ($f < 0.5$), the relatively smaller curvature energy for $\theta = 0^\circ$ suggests that an initially vertically docked or titled ($0^\circ < \theta < 90^\circ$) NP would tend to lay down by rotation, that is, aligning its long axis with the membrane surface. Once the wrapping extent exceeds $f > 0.5$, wrapping with the angle $\theta = 90^\circ$ involves a smaller curvature energy penalty, and hence the NP would tend to stand up to gain a larger wrapping angle θ . Upon completion of rotation, the NP would be wrapped with this angle until it is completely endocytosed. Thus, an initially vertically docked NP would take a laying-down-then-standing-up sequence to complete endocytosis.

To gain a refined picture of the wrapping-rotation sequence, we next perform a local free energy analysis. Endocytosis involves sequential ligand–receptor binding to wrap the NP; each ligand–receptor binding leads to a chemical energy release of $-\mu$ and an increment of the wrapping area of $\Delta f = \xi_1^{-1}$. The thermodynamic driving force ΔE_T for the system going from a wrapped state ($f;\theta$) to the next state ($f + \Delta f;\theta + \Delta\theta$) is

$$\Delta E_T = -\mu + \Delta E_C \quad (1)$$

where

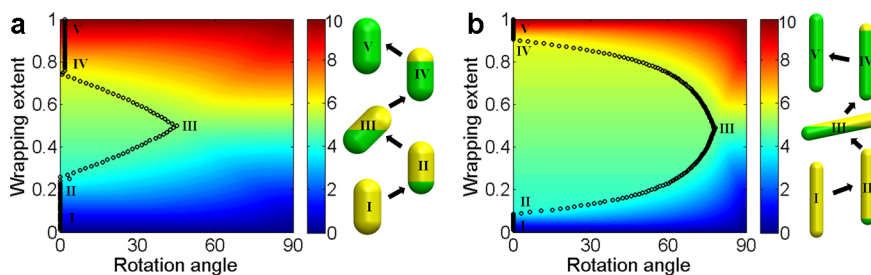


Figure 5. Endocytic pathways for NPs with $\rho = 2$ (a) and $\rho = 5.5$ (b) predicted by local energetics. The spherocylindrical NPs take a general laying-down-then-standing-up sequence during endocytosis. The contour maps plot the curvature energy level in the plane of rotation angle and wrapping extent. The turning points along the endocytic pathways are schematically shown on the right of each subfigure, where the green-shaded areas are wrapped, while the gold-shaded areas are naked.

$$\Delta E_C = E_{,f}(f; \theta)\Delta f + E_{,\theta}(f; \theta)\Delta\theta \quad (2)$$

is the bending energy penalty, and $E_{,f}$ and $E_{,\theta}$ are the first derivatives of the energy with respect to the wrapping extent and angle, respectively. Whether binding is thermodynamically favorable ($\Delta E_T \leq 0$) depends on how discrete the ligand (ξ_1) is on the NP surface as well as the local energy landscape set by the wrapping extent f and the wrapping angle θ . It is possible that the endocytosis is locally stalled ($\Delta E_T > 0$), which may account for the relatively larger minimal R determined by CGMD simulations than the analytical solution obtained from the global energy balance. It should be noted that in the expression of ΔE_C the first term is the curvature energy due to an incremental wrapping area of Δf , while the second term is the energy variation when the wrapping angle is subjected to a small change of $\Delta\theta$. One notes that ΔE_C is always positive (so is $E_{,f}$), since wrapping always needs to pay curvature energy penalty. However, the direction along which the incremental area is wrapped depends on the energy variation associated with $\Delta\theta$. In the case that $E_{,\theta}\Delta\theta < 0$, rotation is energetically favorable. There exist three possibilities for each incremental wrapping: the wrapping angle remains unchanged ($\Delta\theta = 0$); tilted with a positive angle increment ($\Delta\theta > 0$) or with a negative angle increment ($\Delta\theta < 0$), depending on the value of $E_{,\theta}$, that is, the local energy landscape associated with the wrapping angle.

The above local free energy analysis sets a criterion that determines the endocytic pathways of the NPs. We numerically compute the energies of the three possible end states and identify the one with the lowest energy state as the energetically most favorable rotation direction. In the case that no energy difference is found for the three cases, we artificially specify that the NP be wrapped with the previous wrapping direction. Figure 5 plots the endocytic pathways of two representative NPs with $\rho = 2$ (a) and $\rho = 5.5$ (b) in the plane of the rotation angle θ and the wrapping extent f . The pathways are consistent with curvature energy landscapes plotted by the colored contour maps. For both cases, the NPs are initially in the upright docking position with respect to the membrane plane and the endocytic pathway involves a laying-down-then-standing-up sequence, as plotted by the open circles. The turning points along the pathways are schematically shown by the subfigures on the right, where the green-colored portion represents the wrapped area and gold-colored the naked area. With increasing aspect ratio, the laying-down angle increases, i.e., its long axis is nearly parallel to the membrane plane. Both the NPs stand up by rotation from the laying-down position to the upright position before they are fully endocytosed. Extending this observation to the limit of 1D nanorods (such

as long carbon nanotubes),²² endocytosis would involve tip rotation before it completes with a 90° entry angle.

The pathways predicted in Figure 5 captures the general trend of CGMD simulations with some discrepancies. For example, in the CGMD simulations for $\rho = 2$, the NP lays down completely (90° rotation angle), while in our free energy analysis the rotation angle is $\sim 45^\circ$; the entry angle in the CGMD simulations is $\sim 70^\circ$, while our free energy analysis predicts a 90° entry. The discrepancies may arise from the simplification of the CGMD model as well as the lack of the consideration of the kinetics in our free energy analysis. From a kinetics point of view, the amount of curvature energy ΔE_C needs to be paid prior to the chemical energy release via each ligand–receptor binding, representing an energy barrier for the incremental wrapping. During the laying-down process, owing to the relatively high thermodynamic driving force and the very high Reynolds number (because of the solvent-free treatment of the CGMD model), the NPs in the simulations likely gain an angular momentum that drives the rotation of the NPs in the previous rotation directions. This explains the larger rotational angles in the simulations than that predicted in the free energy analysis during the laying-down process. In addition, in the case that all the three wrapping angle variations ($\Delta\theta > 0$; $\Delta\theta = 0$; $\Delta\theta < 0$) are thermodynamically favorable for further wrapping, which wrapping angle the system would take could follow a statistical possibility, instead of deterministically taking place along the direction with the highest thermodynamic driving force, as assumed in our free energy analysis. Further, the curved membrane surface during endocytosis presents difficulties to stabilize the membrane at tensionless condition using the Berendsen barostat in the CGMD simulations. As a result, small residual tension might exist in the membrane, which would deviate the endocytic pathways slightly from those under the tensionless condition.

In conclusion, our CGMD simulations demonstrate that endocytosis of NPs is size dependent and shape sensitive. For long spherocylindrical NPs that are vertically docked on the membrane surface, endocytosis proceeds by a laying-down-then-standing-up sequence. Our free energy analyses show that NP size primarily determines whether endocytosis can complete, while shape breaks the symmetry of the curvature energy landscape and hence dictates the endocytic pathways. We further established under the tensionless condition a local energy criterion with which we map out the detailed endocytic pathways for NPs of different aspect ratios. Extending our results to the limiting case, a 1D nanorod would be endocytosed with a 90° entry angle, which agrees with the tip rotation phenomenon observed in previous studies.²² The

energy criterion for the endocytic pathways may be applicable to NPs with other shapes and can be easily extended to the finite membrane tension condition. In addition to providing a fundamental understanding of the size and shape effects on the endocytosis of NPs, our findings offers useful guidance to engineer NP-bioconjugates for cancer diagnosis and therapy with improved cellular targeting and controlled entry.

■ ASSOCIATED CONTENT

■ Supporting Information

Detailed descriptions on the CGMD model and energetic analyses are provided. This material is available free of charge via the Internet at <http://pubs.acs.org>.

■ AUTHOR INFORMATION

Corresponding Author

*E-mail: suz10@psu.edu.

Present Address

^{||}Disease Biophysics Group, Wyss Institute for Biologically Inspired Engineering, School of Engineering and Applied Science, Harvard University, Cambridge, Massachusetts 02138, U.S.A.

Notes

The authors declare no competing financial interest.

■ ACKNOWLEDGMENTS

S.L.Z. acknowledges support by the National Science Foundation (Grant CMMI-0754463 and CBET-1067523); H.J.G. acknowledges support by the National Science Foundation (Grant CMMI-1028530).

■ REFERENCES

- (1) Douglas, T.; Young, M. *Science* **2006**, *312* (5775), 873–875.
- (2) Lewis, J. D.; Destito, G.; Zijlstra, A.; Gonzalez, M. J.; Quigley, J. P.; Manchester, M.; Stuhlmann, H. *Nat. Med.* **2006**, *12* (3), 354–360.
- (3) Manchester, M.; Singh, P. *Adv. Drug Delivery Rev.* **2006**, *58* (14), 1505–1522.
- (4) Aoyama, Y.; Kanamori, T.; Nakai, T.; Sasaki, T.; Horiuchi, S.; Sando, S.; Niidome, T. *J. Am. Chem. Soc.* **2003**, *125* (12), 3455–3457.
- (5) Gao, X. H.; Cui, Y. Y.; Levenson, R. M.; Chung, L. W. K.; Nie, S. M. *Nat. Biotechnol.* **2004**, *22* (8), 969–976.
- (6) Mornet, S.; Vasseur, S.; Grasset, F.; Duguet, E. *J. Mater. Chem.* **2004**, *14* (14), 2161–2175.
- (7) Michalet, X.; Pinaud, F. F.; Bentolila, L. A.; Tsay, J. M.; Doose, S.; Li, J. J.; Sundaresan, G.; Wu, A. M.; Gambhir, S. S.; Weiss, S. *Science* **2005**, *307* (5709), 538–544.
- (8) Gu, F. X.; Karnik, R.; Wang, A. Z.; Alexis, F.; Levy-Nissenbaum, E.; Hong, S.; Langer, R. S.; Farokhzad, O. C. *Nano Today* **2007**, *2* (3), 14–21.
- (9) Chithrani, B. D.; Ghazani, A. A.; Chan, W. C. W. *Nano Lett.* **2006**, *6* (4), 662–668.
- (10) Chithrani, B. D.; Chan, W. C. W. *Nano Lett.* **2007**, *7* (6), 1542–1550.
- (11) Jiang, W.; Kim, B. Y. S.; Rutka, J. T.; Chan, W. C. W. *Nat. Nanotechnol.* **2008**, *3* (3), 145–150.
- (12) Gratton, S. E. A.; Ropp, P. A.; Pohlhaus, P. D.; Luft, J. C.; Madden, V. J.; Napier, M. E.; DeSimone, J. M. *Proc. Natl. Acad. Sci. U.S.A.* **2008**, *105* (33), 11613–11618.
- (13) Deserno, M.; Bickel, T. *Europhys. Lett.* **2003**, *62* (5), 767–773.
- (14) Gao, H. J.; Shi, W. D.; Freund, L. B. *Proc. Natl. Acad. Sci. U.S.A.* **2005**, *102* (27), 9469–9474.
- (15) Bao, G.; Bao, X. R. *Proc. Natl. Acad. Sci. U.S.A.* **2005**, *102* (29), 9997–9998.
- (16) Sun, S. X.; Wirtz, D. *Biophys. J.* **2006**, *90* (1), L10–L12.
- (17) Zhang, S.; Li, J.; Lykotrafitis, G.; Bao, G.; Suresh, S. *Adv. Mater.* **2009**, *21*, 419–424.
- (18) Yuan, H. Y.; Zhang, S. L. *Appl. Phys. Lett.* **2010**, *96* (3), 033704.
- (19) Yuan, H. Y.; Li, J.; Bao, G.; Zhang, S. L. *Phys. Rev. Lett.* **2010**, *105* (13), 138101–138104.
- (20) Yuan, H. Y.; Huang, C. J.; Zhang, S. L. *PLoS One* **2010**, *5* (10), e13495.
- (21) Yang, K.; Ma, Y. Q. *Nat. Nanotechnol.* **2010**, *5* (8), 579–583.
- (22) Shi, X.; von dem Bussche, A.; Hurt, R. H.; Kane, A. B.; Gao, H. *Nat. Nanotechnol.* **2011**, *6* (11), 714–719.
- (23) Vacha, R.; Martinez-Veracoechea, F. J.; Frenkel, D. *Nano Lett.* **2011**, *11* (12), 5391–5395.
- (24) Yuan, H. Y.; Huang, C. J.; Li, J.; Lykotrafitis, G.; Zhang, S. L. *Phys. Rev. E* **2010**, *82* (1), 011905.
- (25) Cooke, I. R.; Deserno, M. *J. Chem. Phys.* **2005**, *123* (22), 224710.
- (26) Noguchi, H. *J. Phys. Soc. Jpn.* **2009**, *78* (4), 9.
- (27) Quinn, P.; Griffiths, G.; Warren, G. *J. Cell Biol.* **1984**, *98* (6), 2142–2147.
- (28) Briggs, J. A. G.; Wilk, T.; Fuller, S. D. *J. Gen. Virol.* **2003**, *84*, 757–768.
- (29) Chen, Y.; Munteanu, A. C.; Huang, Y.-F.; Phillips, J.; Zhu, Z.; Mavros, M.; Tan, W. *Chem.—Eur. J.* **2009**, *15* (21), 5327–5336.
- (30) Osaki, F.; Kanamori, T.; Sando, S.; Sera, T.; Aoyama, Y. *J. Am. Chem. Soc.* **2004**, *126* (21), 6520–6521.
- (31) Helfrich, W. *Z. Naturforsch.* **1973**, *C 28* (11–1), 693–703.
- (32) Raucher, D.; Sheetz, M. P. *Biophys. J.* **1999**, *77* (4), 1992–2002.